INTERNATIONAL JOURNAL FOR NUMERICAL METHODS IN FLUIDS
*Int. J. Numer. Meth. Fluids* 2000; **33**: 641–656

# Absorbing boundary technique for open channel flows

Scott A. Yost[a,*], Prasada Rao[a] and Russell M. Brown[b]

[a] *Department of Civil Engineering, University of Kentucky, Lexington, KY, U.S.A.*
[b] *Department of Mathematics, University of Kentucky, Lexington, KY, U.S.A.*

## SUMMARY

An absorbing boundary condition is formulated and applied to the one-dimensional open channel flow equations in conjunction with an explicit MacCormack scheme. The physical flow domain has been truncated by introducing an artificial pseudo-boundary. By using an appropriate boundary condition on a truncated domain, it is shown that, for flow containing shocks, the solution can be accelerated to its stationary profile with no loss of accuracy. Copyright © 2000 John Wiley & Sons, Ltd.

KEY WORDS: non-reflecting boundary; open channel flows; shocks; subcritical/supercritical flow

## 1. INTRODUCTION

Numerical modeling of flow in open channels often involves computational domains that are very large. Discretizing the entire computational domain and solving the flow equations turns out to be a tedious task, both in terms of computational time and the corresponding memory requirements. For flows where steady state solutions are sought, the large domain taxes the computational resources, as the steady state profiles are obtained by solving the time-dependent flow equations over a large time period. In this approach, which is also known as the false transient approach, time is used as an iteration parameter. To alleviate the above problems an alternative is to translate the known boundary condition onto a pseudo boundary, which results in a smaller computational domain. Decreasing the size of the computational domain helps in accelerating the convergence of the solution to steady state. Figure 1 illustrates the above discussion. The total flow domain $\Omega$ of length $L$ is truncated by placing an artificial boundary (B–B) at length $L_1$ from the upstream boundary. The effectiveness of such an approach primarily depends on how well the boundary condition at B–B relates to the physical boundary at A–A.

This paper begins by discussing the boundary conditions at section A–A before relating them to those at section B–B. Specifying proper boundary conditions is an important aspect

* Correspondence to: Department of Civil Engineering, University of Kentucky, 161 Oliver H. Raymond Building, Lexington, KY 40506-0281, U.S.A.



*Received 26 August 1998*
*Revised 18 August 1999*

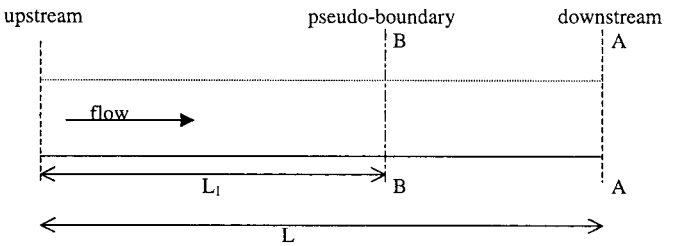


Figure 1. Schematic representation of the new flow domain.

in any numerical investigation. Overspecifying or underspecifying the flow variables will result in incorrect flow values [1,2]. The exact number of boundary conditions to be specified at the end nodes depends on the nature of the flow. By using the method of characteristics, one can show that for supercritical flows ($F_r > 1$, with $F_r$ indicating the Froude number), all flow information needs to be specified upstream (Figure 2). Hence, for one-dimensional computations the two flow variables are specified at the upstream end and none at the downstream end [2]. The variables at the downstream end are obtained by interpolating them from interior nodes. For subcritical flows ($F_r < 1$), one boundary condition at both the upstream and the downstream ends need to be specified. The other variable is compared using the relevant characteristic equation. The number of boundary conditions required for different flow configurations is documented in Table I.

In this investigation, the focus is on steady profiles for flows accompanied with shocks, as these are considered to be critical in testing the effectiveness of the absorbing boundary condition at section B–B [3–5]. Shocks in open channels, broadly known as hydraulic jumps, arise whenever supercritical flow reverts to subcritical flow (see Figure 3). Because the flow is subcritical at the downstream end of the physical domain, one flow condition needs to be specified. An ideal boundary condition at B–B should satisfy the following criteria: (i) the boundary condition should be compatible with the physics of the problem, (ii) the new boundary should not degrade the solution, and (iii) the boundary should absorb the outgoing wave to avoid any waves being reflected back into the flow domain. Failure to satisfy the first two conditions could result in an incorrect solution. A reflecting boundary (violating condition (iii)) could result in a larger number of computational steps for the disturbance to be

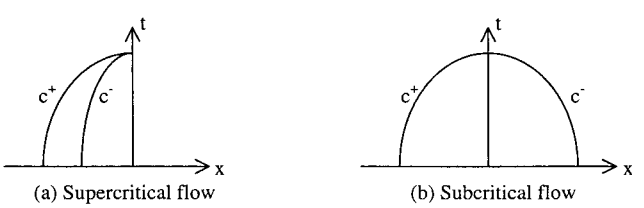


Figure 2. Characteristic curves in $x$-plane.

 

Table I. Nature of flow and required boundary conditions.

| Location | One-dimensional flows | | Two-dimensional flows | |
|---|---|---|---|---|
| | Subcritical | Supercritical | Subcritical | Supercritical |
| Upstream | 1 | 2 | 2 | 3 |
| Downstream | 1 | 0 | 1 | 0 |

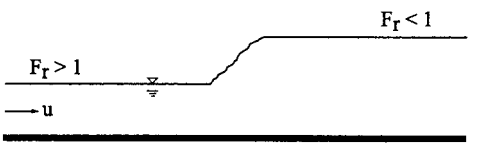


Figure 3. Schematic representation of hydraulic jump.

dissipated. The length at which the boundary B–B is placed (i.e., $L_1$) needs a special mention. For example, if the flow conditions dictate the formation of stationary discontinuity at a distance $L_2$ from the upstream end, then in the process of truncating the flow domain, the boundary B–B should be placed beyond $L_2$ from the upstream end. In addition, to maintain the accuracy of the solution, the boundary B–B should be placed some distance away from the discontinuity region. In particular, the gradients of flow variables near the boundary should be small. The placement of the artificial boundary is covered in greater detail below (see the discussion relating to Figure 5).

The objective of the this work is to obtain a satisfactory radiating boundary equation, also known as a 'non-reflecting' or 'absorbing' boundary condition, for open channel flow equations. The use of an appropriate boundary condition at the pseudo-boundary aids in reducing the size of the computational domain, thus accelerating the solution to steady state. It should allow the wave to propagate outside of the computational domain without generating any reflections back into the domain. A satisfactory equation yields an approximate solution in the truncated domain, coinciding with the exact solution over the unbounded domain. In deriving the absorbing boundary equation, use has been made of the structure of the outgoing wave and a normal mode analysis [3]. To the knowledge of the authors, no other work has been done in the field of computational hydraulics, thus they present the derivation of the absorbing equation for these flow equations in greater detail. Finally, to make this document self-contained, all numerical aspects are briefly presented.

## 2. GOVERNING EQUATIONS

For a rectangular channel, the basic governing equation based on the continuity and momentum principles can be written in conservation form as [2]

 

$$h_t + (hu)_x = 0 \tag{1}$$

$$(hu)_t + \left(hu^2 + \frac{gh^2}{2}\right)_x = gh(S_0 - S_f) \tag{2}$$

where $h$ is the flow depth, $u$ is the flow velocity, $g$ is the acceleration due to gravity, $S_0$ is the bed slope of the channel and $S_f$ is the frictional slope, computed using Manning's equation and written as

$$S_f = \frac{m^2 u|u|}{R^{4/3}} \tag{3}$$

Here $m$ is the Manning roughness coefficient and $R$ is the hydraulic radius (ratio of area of flow to wetted perimeter). The definition sketch identifying some of the flow variables is illustrated in Figure 4.

## 3. NUMERICAL SCHEME

Since we are focussing on boundary issues, we have selected the established finite difference MacCormack scheme for solving Equations (1) and (2). Note that any shock capturing scheme from the family of total variation diminishing (TVD) or essentially non-oscillatory (ENO) schemes can be used since the present boundary formulation is independent of the numerical technique. With the application of the MacCormack scheme to free surface flows being well documented [2,6,7], we only outline the smoothing procedure that has been used to stabilize the solution near the shock [8]. This smoothing technique, which is also known as 'artificial viscosity', aids in arriving at a smooth profile. Since we are using the MacCormack scheme, we have used the procedure originally suggested by Jameson *et al.* [9]. In this approach, the flow variable ($f$ in this discussion, which can be depth or discharge) is smoothed as

$$f_i^{n+1} = f_i^{n+1} + \xi_{i+1/2}(f_{i+1}^{n+1} - f_i^{n+1}) - \xi_{i-1/2}(f_i^{n+1} - f_{i-1}^{n+1}) \tag{4}$$

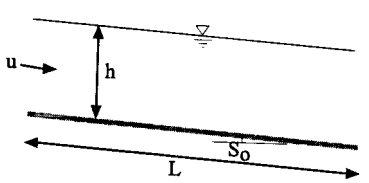


Figure 4. Definition sketch.

 

where

$$\xi_i = \frac{|h_{i+1} - 2h_i + h_{i-1}|}{|h_{i+1}| + 2|h_i| + |h_{i-1}|} \tag{5}$$

$$\xi_{i+1/2} = \mu \max(\xi_i, \xi_{i+1}) \tag{6}$$

The solution obtained by Equation (4) is free from any oscillations. The smoothing mechanism (Equation (5)) is triggered only in oscillatory regions. For regions where the flow is uniform, the numerator in Equation (5) goes to zero, leaving the solution undistributed. The parameter $\mu$ in Equation (6) is a dissipation constant that controls the degree of smoothing. The magnitude of which is determined by numerical testing.

The choice of time step is governed by the Courant–Friedrich–Lewy (CFL) stability condition [10], and is given by

$$\Delta t = C_n \frac{\Delta x}{\max(|u| + \sqrt{gh})} \tag{7}$$

where $C_n$ is the Courant number, and $\Delta x$ is the grid spacing. With known grid spacing and flow conditions, the time step can be evaluated using Equation (7).

## 4. TEST PROBLEM

Before moving the discussion to the formulation of the appropriate absorbing equation at section B–B (see Figure 1), we present the salient features of the test problem. As mentioned, the proposed formulation has been tested for flow accompanied with discontinuities. In an open channel flow application, this includes hydraulic jumps. Due to its practical importance, numerical simulation of hydraulic jumps continues to draw the research interest of modelers in the hydraulic community [2,11–13].

The experimental results of Gharangik and Chaudhry [11] have been used as our benchmark solution. The initial conditions in the 14 m long horizontal channel ($S_0 = 0$) are a flow depth of 0.043 m and a flow velocity of 2.737 m s$^{-1}$. These flow conditions result in a Froude number ($F_r$) of 4.23. At time $t = 0^+$, the unsteady computations are started by increasing the depth at the downstream end (similar to closing a gate) to 0.22 m, and the simulation continued until the solution converges to steady state for these flow conditions. This particular combination of flow conditions causes a hydraulic jump where the flow changes from supercritical ($F_r > 1$) to subcritical ($F_r < 1$).

All the studies reported [11–13] have simulated this problem by solving the flow equations over the entire domain (i.e., channel length of 14 m). In the present work, the flow domain is truncated to half of the original length ($L_1 = 7$ m), and an appropriate absorbing boundary condition was placed at this new downstream boundary. The equation that relates the flow variables at these two boundaries is known as the absorbing boundary condition, which is derived next.

 

## 5. ABSORBING EQUATION

At the outset we note that the mathematical theory for hyperbolic conservation laws is not completely understood (see Reference [5], p. 438). In particular, we do not know if uniqueness can be established for the boundary condition (Equation (8)) derived below. Thus, we rely on heuristic techniques and computational results to justify this boundary condition. Next, we note that we are interested in the case when the Froude number at the artificial boundary is less than one. Thus, we need to impose one boundary condition there. The boundary condition that we use is

$$h_t - \frac{c}{g} u_t + \alpha(h - \bar{h}) = -c(S_0 - S_f) \tag{8}$$

where $c = \sqrt{gh}$ is the celerity of the wave and $\alpha$ is a parameter to be chosen, as discussed below.

Justification in the use of Equation (8) in the light of the properties it should possess (see Section 1) can be obtained from the work of Engquist and Majda [14]. Starting the discussion from the lowest level of abstractness, Hedstrom [15] gives the following boundary condition (written for our problem), which is similar to Equation (8):

$$h_t - \frac{c}{g} u_t = -c(S_0 - S_f) \tag{9}$$

This is plausible because the quantity $h - (cu)/g$ is the characteristic variable for the outgoing wave. However, Equation (9) is not useful because it does not incorporate the downstream height $\bar{h}$. The equation provided by Rudy and Strikwerda [3] incorporates this information by appending the term $\alpha(h - \bar{h})$. They attempt to choose a value of $\alpha$ by taking the system of equations in non-conservation form, freezing the Jacobian at constant values and examining the exponential solutions for the resulting system. If one considers the following:

$$\hat{h} = h - \bar{h}, \qquad \hat{u} = u - \bar{u} \tag{10}$$

with the boundary conditions

$$\hat{u}(0, t) = 0 \tag{11}$$

and

$$\hat{h}_t = (L^*, t) - \sqrt{\frac{\bar{h}}{g}}\, \hat{u}_t(L^*, t) + \alpha \hat{h} = 0 \tag{12}$$

then, according to Rudy and Strikwerda, the most rapid decay is achieved if

 

$$\alpha = \frac{c^2 - \bar{u}^2}{3.59cL^*} \tag{13}$$

The choice of $L^*$ in our investigation was based on the maximum length of the interval where $u = \bar{u}$ and $h = \bar{h}$ are valid. In the numerical code, this was achieved by keeping track of the shock profile evolution as a function of time and grid node. Having tracked the location of the discontinuity, $L^*$ is the length of the channel between the discontinuity and the downstream end. This is the maximum length where the flow tends to be uniform so that $\hat{u}$ and $\hat{h}$ are small. Even for flows with shocks there exists a substantial flow domain where the flow variables are close to constant. The basic assumption of flow in this region is that the pressure distribution is hydrostatic. Basco [16] has numerically shown that the contribution of non-hydrostatic pressure distribution is significant only in the regions containing the shock and is minimal in regions away from it. The numerical results of Gharangik and Chaudhry [11] and Rahman and Chaudhry [12] also substantiate the above statement.

Note that Rudy and Strikwerda's equation is not yet appropriate for our problem. This is because Equation (12) is not satisfied by the steady state solution since for our case $\hat{h} = (h - \bar{h}) \neq 0$. Thus, we observe that the right-hand term of momentum equation (Equation (2)) is a slope term. Hence, one could expect

$$(h - \bar{h}) = -\tilde{L}(S_0 - S_f) \tag{14}$$

Adding this heuristic boundary condition gives $\alpha = c/\tilde{L}$, where $\tilde{L}$ is the distance from artificial to physical boundaries ($\tilde{L} = L - L_1$ in Figure 1). The celerity, $c$, is introduced to make the equation dimensionally homogenous.

We remark that a different explanation for the right-hand side can be given by considering the linearized system

$$\begin{pmatrix} \hat{h} \\ \hat{u} \end{pmatrix}_t + \begin{pmatrix} \bar{u} & \bar{h} \\ g & \bar{u} \end{pmatrix} \begin{pmatrix} \hat{h} \\ \hat{u} \end{pmatrix}_x = \begin{pmatrix} 0 \\ F \end{pmatrix} \tag{15}$$

where $g(S_0 - S_f)$ is assumed to be constant, denoted by $F$. Then, the solutions of this system are easily seen to be

$$\begin{pmatrix} \hat{h} \\ \hat{u} \end{pmatrix} = \varphi_+(x - C^+ t) \begin{pmatrix} \sqrt{h/g} \\ 1 \end{pmatrix} + Ft + \varphi_-(x - C^- t) \begin{pmatrix} \sqrt{\bar{h}/g} \\ -1 \end{pmatrix} \tag{16}$$

where $\varphi_+$ and $\varphi_-$ are arbitrary real functions. If we assume that for the incoming wave, $\varphi_- = 0$, then the solution satisfies the boundary condition

$$\hat{h}_t - \sqrt{\frac{\bar{h}}{g}}\,\hat{u}_t = -\sqrt{\frac{\bar{h}}{g}}\,F = -c(S_0 - S_f) \tag{17}$$

Now adding the term $\alpha(h - \bar{h})$ gives the boundary condition found in Equation (8).

 

## 6. APPLICATION

As mentioned before, we have selected flows with shocks to validate the present formulation. Since the location of discontinuity is sensitive to the boundary condition, we feel this type of flow serves as a critical code validation test for the radiating boundary equation. A grid spacing of 0.23 m, Manning's roughness coefficient of 0.0085, a Courant number of 0.4, and a dissipation constant ($\mu$ in Equation (6)) of 0.5 were used in this investigation. Readers who are interested in the experimental methodology are referred to Gharangik and Chaudhry [11].

Since the flow is supercritical at the upstream end ($x = 0$), the flow variables were kept constant at their initial values. At the downstream end the boundary conditions could be applied in one of three ways, including

1. extrapolation of flow variables from the interior node;
2. using a constant flow depth, compute the velocity using the $C^+$ curve from the governing equation; or
3. using the proposed non-reflection equation (Equation (8)).

The physics of the problem dictate that one flow variable must be specified at the downstream end; hence the first approach is incorrect. The second approach is valid in a subcritical flow simulation. The information that is supplied by the $C^-$ curve is replaced with the known flow variable or physical relation. However, when we truncate the flow domain, we do not know the flow information at the new downstream end (i.e. section B–B in Figure 1). Had the steady state solution been known a *priori* (which is never the case), the second approach can be applied at our new boundary. Equating the value of flow variables at the end of the physical domain (at $x = L$) to the pseudo-boundary (at $x = L_1$) is inconsistent and could lead to incorrect solutions. Hence, an appropriate boundary value at the pseudo-boundary is needed. We use Equation (8) to determine it. It should be noted that the linearized equations were solved only at the boundary node, and the conservation form of the equations (Equations (1) and (2)) was solved over the rest of the domain. In the following discussion, the flow was assumed to have reached steady state if

$$\sum_{i=1}^{\mathrm{NG}} \frac{1}{\mathrm{NG}} \sqrt{(h_i^{n+1} - h_i^n)^2} \leq \varepsilon = 10^{-9} \tag{18}$$

with NG indicating the total number of grid nodes in the computational domain.

Figure 5 shows the location of the steady state profile with and without the absorbing boundary. When computing the profile without the absorbing boundary equation, the downstream boundary was placed at $x = L = 14$ m. Coupled with the given boundary depth of 0.043 m, the flow velocity was computed using the $C^+$ equation of Equations (1) and (2). If $K$ represents the last grid note, the $C^+$ equation can be written as [2]

$$u_K^{n+1} = u_{K-1}^n - \frac{8}{\sqrt{g h_{K-1}^n}} (h_K^{n+1} - h_{K-1}^n) - g \Delta t S_{\mathrm{f}} \tag{19}$$

 

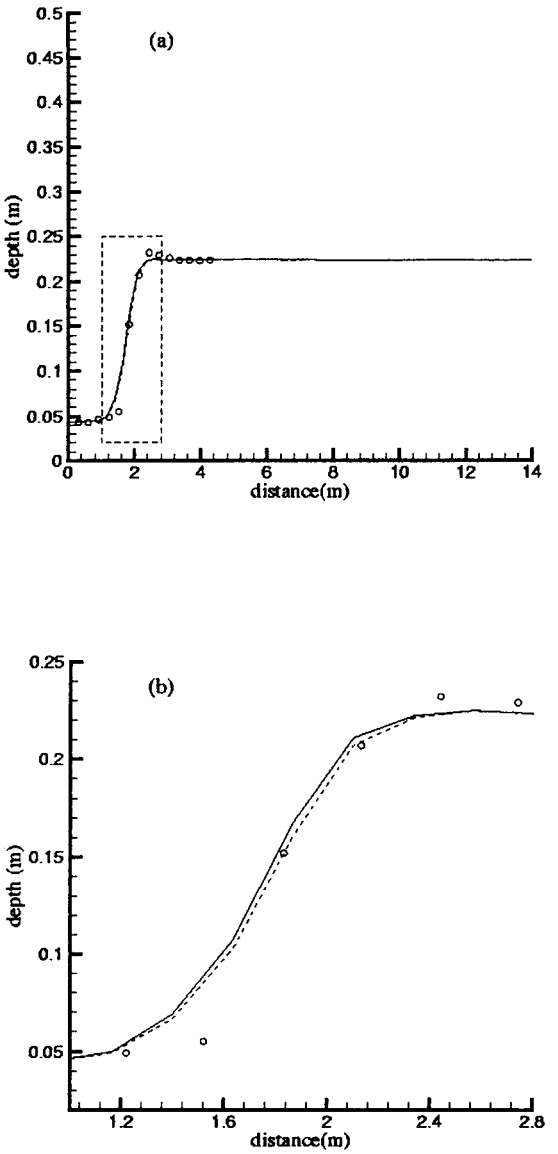


Figure 5. Steady state profiles for $F_r = 4.23$: (a) normal view; (b) zoom view, — without absorbing boundary ($L_1 = 14$ m), – – – with absorbing boundary ($L_1 = 7$m); ○, experimental [11].

To test the efficiency of the absorbing boundary condition the flow domain was truncated to $x = L_1 = 7$ m. The boundary condition (i.e., known flow depth at 14 m) was translated to the new boundary using Equation (8). Figure 5 indicates that the flow profile obtained using the present absorbing boundary equation is in close agreement with the characteristic solution of the whole domain. As previously mentioned, constricting the size of the flow domain aids in reducing the computational effort and expense. In addition, the close agreement of the absorbing solution with the experimental data reinforces the reliability of Equation (8). The steady state value of $\alpha$, as obtained using Equation (13), was 0.216. Taking this magnitude as the base value we varied $\alpha$ by $\pm 50\%$ and performed the simulation again. The sensitivity of the profiles to $\alpha$ is plotted in Figure 6. The plot shows that lower values of $\alpha$ tend to give an incorrect location of the discontinuity. Figure 7 is the plot of relative error (RE) as a function of $\alpha$. When computing the RE we had taken the solution obtained by running the code over the whole domain ($L_1 = 14$ m) as the base solution, since we did not know the analytical solution. Extensive runs conducted for values of $\alpha$ above that given by Equation (13) ($\alpha > 0.216$) did not affect the location of the stationary discontinuity. Hence, we conclude that Equation (13) gives that threshold value of $\alpha$. Furthermore, varying $\alpha$ had no effect on the spurious oscillations that rise near the discontinuity. As previously mentioned, these oscillations are a characteristic feature of the numerical scheme and are not related to the absorbing boundary condition. In conjunction with Equation (13), we have mentioned that the other possible values of $\alpha$ are given as $\alpha = c/\tilde{L}$. Since for the present investigation, $\tilde{L} = 7$m and $c = 1.47$ m s$^{-1}$ ($\sqrt{g\bar{h}}$), the magnitude of $\alpha$ is equivalent to 0.21.

When plotting Figure 5, we had placed the pseudo-boundary at $x = 7$ m. We had selected this length based on the assumption that the steady state hydraulic jump is located within the first 7 m. If this assumption is wrong and the discontinuity is located outside $L_1$, the present methodology fails to generate a reliable result. Selecting an appropriate truncated domain is difficult, as the steady state solution is not known *a priori*. Thus, a better mechanism is required for determining the length at which the flow domain can be truncated. Had the location of the steady state jump been known before hand, then the selecting a suitable $L_1$ turns out to be an easier task. Given all boundary conditions, the choice of appropriate $L_1$ is elusive. Solving the idealized linear equations will produce a location for the stationary wave. However, the presence of the non-linear source term makes such an approach a difficult task. We are not aware of any analytical approach that can be used for determining the optimum length of $L_1$. Hence, we see this as a limitation in implementing an absorbing boundary condition.

The effect of the Courant number on the location of the shock front is summarized in Table II. The interest was confined to the regions in the vicinity of the discontinuity. The numbers indicate that for a wide range of Courant numbers, the jump forms between 1.63 and 1.866 m. Computations were made for different flow conditions (i.e., Froude numbers) to observe a similar trend as indicated in Figures 5–7 and Table II. To conserve space, we have presented the results of one flow condition.

Finally, we apply the absorbing boundary technique for channels with non-rectangular cross-section to illustrate the applicability to more general channels. Specifically, channels with trapezoidal and triangular cross-sections are used. The continuity and momentum equations for the channels of interest can be written as

 

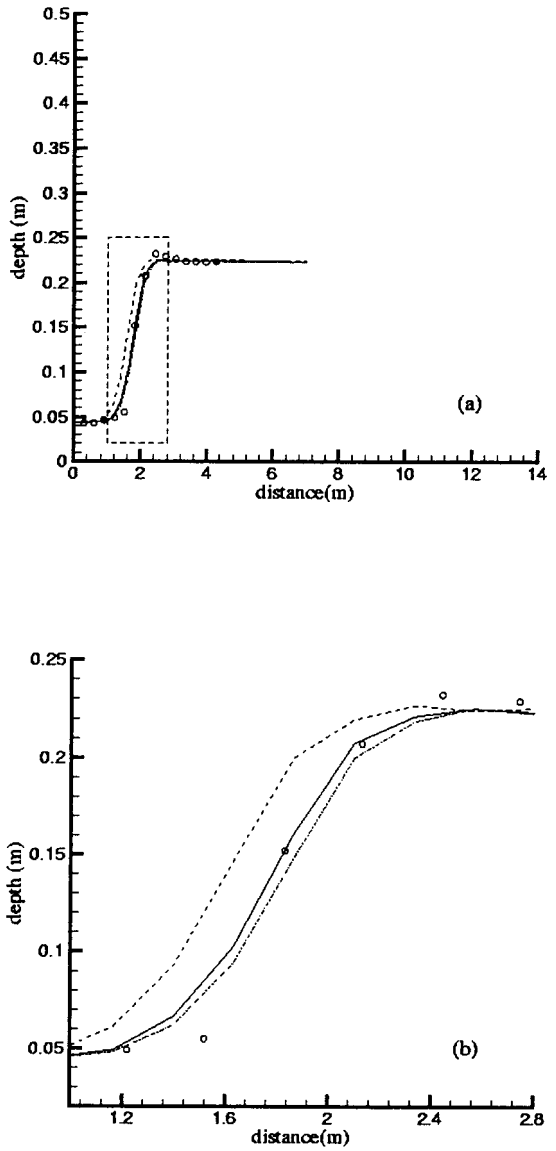


Figure 6. Effect on $\alpha$ on the location of jump: (a) normal view; (b) zoom view, — $\alpha = 0.22$ (Equation (13)), – – $\alpha = 0.11$, – · – 0.32; ○, experimental [11].

$$A_t + Q_x = 0 \tag{20}$$

$$Q_t + \left(\frac{Q^2}{A} + gI\right)_x = gA(S_0 - S_f) \tag{21}$$

 

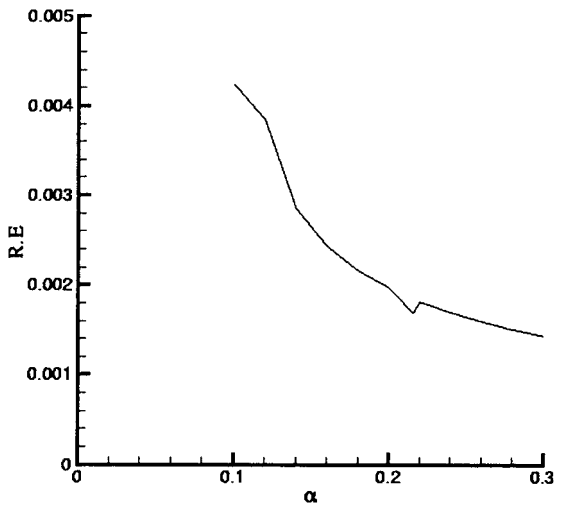


Figure 7. Effect of $\alpha$ on RE.

Table II. Effect of Courant number on shock location.

| $Cn \downarrow$ $x \rightarrow$ | 1.16 | 1.40 | 1.63 | 1.866 | 2.10 |
|---|---|---|---|---|---|
| 0.1 | 5.2E−2 | 6.7E−2 | 9.6E−2 | 0.14 | 0.18 |
| 0.4 | 4.9E−2 | 6.6E−2 | 1.0E−2 | 0.16 | 0.20 |
| 0.7 | 5.0E−2 | 7.6E−2 | 0.12 | 0.19 | 0.21 |
| 0.9 | 5.0E−2 | 7.9E−2 | 0.13 | 0.20 | 0.22 |

where $A$ is the wetted cross-sectional area, $Q$ is the flow rate, $I$ is the hydrostatic pressure force, $g$ is the acceleration due to gravity, $S_0$ is the bed slope, and $S_f$ is the friction slope. The hydrostatic pressure force can be expressed as

$$I = \int_0^{h(x,\,t)} (h - \eta) b(x, \eta)\, \mathrm{d}\eta \tag{22}$$

where in $h$ is the water depth, $\eta$ is the integration variable indicating distance from the channel bottom, and $b(x, \eta)$ is the channel width at distance $\eta$ from the channel bottom

$$b(x, \eta) = \frac{\partial A(x, \eta)}{\partial \eta} \tag{23}$$

Using the method of characteristics, one can show that the outgoing wave for Equations (20) and (21) has the form [2]

 

$$h_t - \frac{c}{g} u_t = -c(S_0 - S_f) \tag{24}$$

where the celerity of the wave is $c = \sqrt{gA/T}$, in which $T$ is the top width of the flow. For channels with a rectangular cross-section, Equation (24) is identical to Equation (17), and $c = \sqrt{gh}$. At this stage we like to note that the absorbing boundary formulation is solely dependent on the form of the outgoing wave. Given the fact that Equations (17) and (24) are similar, the discussion presented in Section 5 can be extended to any cross-sectional channel. Hence, one can arrive at the appropriate boundary equation at the pseudo-downstream end by adding the term $\alpha(h - \bar{h})$ to the left-hand side of Equation (24). Numerical verification shows this to be true.

The geometric features of the trapezoidal cross-sectional channel are channel length = 14 m, bottom width = 0.5 m, side slope = 1:1, and roughness coefficient = 0.0155. The initial conditions are a flow depth, $h = 0.043$ m and discharge, $Q = 0.053$ m$^3$ s$^{-1}$. These flow conditions result in an upstream Froude number of 4.0. The hydraulic jump was created by increasing the flow depth at the downstream end at $t = 0^+$ to 0.122 m. To check the present formulation we had compared the flow profiles with and without the absorbing boundary. In the former case, the solution was computed for the whole domain at all time periods. When using the absorbing boundary, the domain was truncated at $x = 7$ m and Equation (8) applied at this pseudo-downstream boundary. Figure 8 depicts the depth profiles for the two simulations. The magnitude of $\alpha$ at steady state, given by Equation (13) was 0.0711. The close agreement between the two profiles indicates that the cross-sectional shape is no limitation for applying the absorbing equation.

The initial conditions in the triangular channel are a flow depth, $h = 0.1$ m and discharge, $Q = 0.023$ m$^3$ s$^{-1}$. These conditions resulted in a Froude number of 5.4. The depth at the downstream end at $t = 0^+$ was increased to 0.3. The slope of the channel sides in the 14 m long horizontal channel is 0.6:1 (i.e., 0.6 horizontal to 1 vertical). A value of 0.015 was used as the Manning roughness coefficient, and the Courant number was set to 0.8. Figure 9 illustrates the depth profiles obtained with and without truncating the domain. In the latter, the domain was truncated at $x = 7$ m. The close agreement between the two profiles reinforces the previous conclusion. Since the channels is real world are often non-rectangular, we hope that the present study will stimulate the interest of absorbing boundary techniques among hydraulic modelers.

We conclude this discussion by sharing our thoughts on extending the present application to higher-dimensional flows. For many problems, an accurate simulation requires solving two- and three-dimensional open channel flow equations. Numerical studies have been reported for flow in a converging/diverging channel, flow in bends and flow over a spur dyke. The application of an absorbing boundary equation depends primarily on the nature of flow at the downstream end (given by the local Froude number) and on the geometry of the truncated domain. We assume that the flow is subcritical downstream because supercritical flow dictates that any downstream boundary equation/condition is invalid due to the upstream control. Additionally, the physical geometry in the truncated domain is assumed to be regular. All the above mentioned flows have a localized irregular domain, wherein the

 

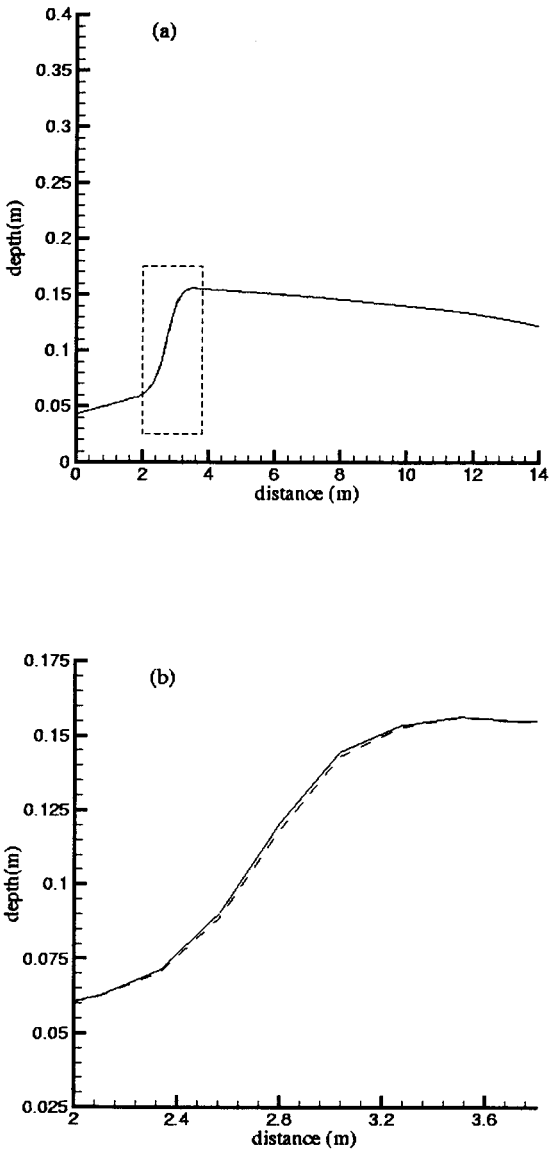


Figure 8. Steady state profiles for trapezoidal channel ($F_r = 4.0$): (a) normal view, (b) zoom view, — without absorbing boundary ($L_1 = 14$ m), – – – with absorbing boundary ($L_1 = 7$ m).

flow is strongly two-dimensional, and a fairly large regular domain wherein the geometry contributes little to the physics of flow. Noting this, the researchers who have studied these flows [13,17,18] have assumed the flow downstream to be one-dimensional. With this

 

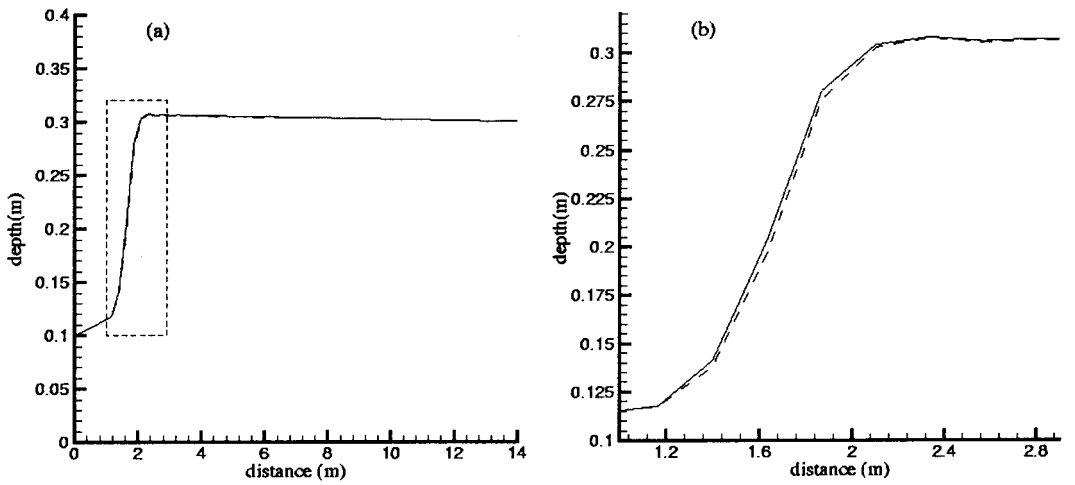


Figure 9. Steady state profiles for triangular channel ($F_r = 5.4$): (a) normal view; (b) zoom view, — without absorbing boundary ($L_1 = 14$ m), – – – with absorbing boundary ($L_1 = 7$ m).

hypothesis, their results are in close agreement with the experimental results. Correlating their findings to this work, the extension to multi-dimensional applications seems somewhat straightforward, but is left for future research.

## 7. CONCLUSIONS

For a set of one-dimensional open channel flow equations with source terms, this paper deals with the application of an absorbing boundary condition. The associated boundary equation transfers the flow information from the actual physical boundary to a pseudo-boundary located within the flow domain. The applicability of this procedure was tested on flows with discontinuities. The observed results are in agreement with numerical and reported experimental results. The use of the absorbing boundary leads to a faster convergence of the solution to steady state, while leaving the location of the stationary wave undisturbed. The limitations in this formulation are (i) the location of the pseudo-boundary must be assumed independent of the steady state location of the discontinuity, and (ii) the geometry of the domain in the truncated region has no significant effect on the solution (i.e., pseudo-one-dimensional). The approach outlined in this work will be explored for higher-dimensional flows in future work.

ACKNOWLEDGMENTS

Russell M. Brown was supported in part by a grant from the National Science Foundation, DMS-9801276. The authors would like to thank anonymous reviewers for their suggestions and ideas, which resulted in them improving the coherency and quality of the manuscript.

 

## REFERENCES


1. Hirsch C. *Numerical Computation of Internal and External Flows*. Wiley: New York, 1992.
2. Chaudhry MH. *Open Channel Flow*. Prentice Hall: New York, 1993.
3. Rudy DH, Strikwerda JC. A non reflecting outflow boundary condition for subsonic Navier–Stokes calculations. *Journal of Computational Physics* 1980; **36**: 55–70.
4. Bayliss A, Turkel E. Outflow boundary conditions for fluid dynamics. *SIAM Journal of Science and Statistical Computing* 1982; **2**: 250–259.
5. Godlewski E, Raviart PA. *Numerical Approximation of Hyperbolic Systems of Conservation Laws*. Springer: New York, 1996.
6. Fennema RJ, Chaudhry MH. Explicit numerical schemes for unsteady free surface flows with shocks. *Water Resources and Research* 19863; **22**: 1923–1930.
7. Garcia R, Kahawita RA. Numerical solution of the St. Venant equations with the MacCormack finite difference scheme. *International Journal for Numerical Methods in Fluids* 1986; **6**: 259–274.
8. Anderson DA, Tannehill JC, Pletcher RH. *Computational Fluid Mechanics and Heat Transfer*. McGraw-Hill: New York, 1984.
9. Jameson A, Schmidt W, Turkel E. Numerical solutions of the Euler equations by finite volume methods using Runge–Kutta time stepping schemes. AIAA 14th Fluid and Plasma Dynamics Conference, Palo Alto, CA. AIAA, , 1981; 81–1259.
10. Courant R, Friedrichs K, Lewy H. ber die Partiellen Differenzengleichungen der Physik. *Mathematical Annals* 1928; **110**: 32–74.
11. Gharangik AM, Chaudhry MH. Numerical simulation of hydraulic jump. *Journal of Hydraulic Engineering ASCE* 1991; **117**: 1195–1211.
12. Rahman M, Chaudhry MH. Simulation of hydraulic jump with grid adaptation. *Journal of Hydraulic Research* 1995; **33**: 555–569.
13. Molls T, Molls F. Space time conservation method applied to Saint Venant equations. *Journal of Hydraulic Engineering ASCE* 1998; **124**: 501–508.
14. Engquist E, Majda A. Absorbing boundary conditions for the numerical simulations of waves. *Mathematics in Computers* 1977; **31**: 629–652.
15. Hedstrom GW. Non-reflecting boundary conditions for nonlinear hyperbolic systems. *Journal of Computational Physics* 1979; **30**: 222–237.
16. Basco DR. Limitations of de Saint Venant equations in dam-break analysis. *Journal of Hydraulic Engineering ASCE* 1989; **115**: 950–956.
17. Dammuller DC, Bhallamudi SM, Chaudhry MH. Modeling of unsteady flow in curved channel. *Journal of Hydraulic Engineering ASCE* 1989; **115**: 1479–1495.
18. Rahman M, Chaudhry MH. Computation of flow in open-channel transition. *Journal of Hydraulic Research* 1997; **35**: 243–256.


 